

Rapid Functional Maturation of Nascent Dendritic Spines

Karen Zito,^{1,3,*} Volker Scheuss,^{1,4} Graham Knott,² Travis Hill,³ and Karel Svoboda^{1,5}

¹Howard Hughes Medical Institute, Cold Spring Harbor Laboratory, Cold Spring Harbor, NY 11724, USA

²Interdisciplinary Centre for Electron Microscopy, Ecole Polytechnique Fédérale de Lausanne, 1015 Lausanne, Switzerland

³Center for Neuroscience, University of California, Davis, Davis, CA 95618, USA

⁴Department of Cellular and Systems Neurobiology, Max-Planck-Institute for Neurobiology, Am Klopferspitz 18, D-82152 Martinsried, Germany

⁵Janelia Farm Research Campus, Howard Hughes Medical Institute, Ashburn, VA 20147, USA

*Correspondence: kzito@ucdavis.edu

DOI 10.1016/j.neuron.2008.10.054

SUMMARY

Spine growth and retraction with synapse formation and elimination plays an important role in shaping brain circuits during development and in the adult brain, yet the temporal relationship between spine morphogenesis and the formation of functional synapses remains poorly defined. We imaged hippocampal pyramidal neurons to identify spines of different ages. We then used two-photon glutamate uncaging, whole-cell recording, and Ca^{2+} imaging to analyze the properties of nascent spines and their older neighbors. New spines expressed glutamate-sensitive currents that were indistinguishable from mature spines of comparable volumes. Some spines exhibited negligible AMPA receptor-mediated responses, but the occurrence of these “silent” spines was uncorrelated with spine age. In contrast, NMDA receptor-mediated Ca^{2+} accumulations were significantly lower in new spines. New spines reconstructed using electron microscopy made synapses. Our data support a model in which outgrowth and enlargement of nascent spines is tightly coupled to formation and maturation of glutamatergic synapses.

INTRODUCTION

The growth and retraction of dendritic spine synapses has been proposed to underlie experience-dependent changes in brain circuitry during development and in the adult brain (Alvarez and Sabatini, 2007; Bailey and Kandel, 1993; Yuste and Bonhoeffer, 2001) and also might play a role in neurodevelopmental disorders (Fiala et al., 2002). Dendritic spines are highly dynamic during development: they grow and retract, elongate and shorten, and change volume and shape (Bonhoeffer and Yuste, 2002; Jontes and Smith, 2000; Matus, 2005; Segal, 2005). Spine dynamics are sensitive to sensory experience (Holtmaat et al., 2006; Lendvai et al., 2000; Majewska and Sur, 2003; Trachtenberg et al., 2002; Zuo et al., 2005), and new spines grow in response to plasticity-inducing synaptic stimuli (Engert and

Bonhoeffer, 1999; Jourdain et al., 2003; Maletic-Savatic et al., 1999; Nagerl et al., 2004). These observations suggest that spine structural changes are associated with adaptive functional changes in cortical circuits.

A role for spine dynamics in circuit plasticity requires that spine morphological changes be associated with changes in synaptic strength or connectivity. Indeed, spine enlargement and shrinkage are associated with increases and decreases in synaptic strength (Matsuzaki et al., 2004; Zhou et al., 2004), and new spine growth is often associated with synapse formation (Bresler et al., 2001; Holtmaat et al., 2006; Knott et al., 2002; Okabe et al., 2001; Trachtenberg et al., 2002; Zito et al., 2004; Ziv and Smith, 1996). Retrospective serial section electron microscopy (SSEM) of previously imaged spines provided anatomical evidence that spine growth in fact precedes synapse formation in vivo in the adult rat neocortex (Knott et al., 2006) and in cultured hippocampal brain slices (Nagerl et al., 2007). These studies suggest a long delay between spine growth and synapse formation (>15 hr). In contrast, experiments in dissociated cultured neurons found that synaptic molecules cluster at nascent synapses only minutes after contact between pre- and postsynaptic elements (Bresler et al., 2001; Friedman et al., 2000; Okabe et al., 2001; Washbourne et al., 2002; Ziv and Smith, 1996). The time course over which functional synapses form on individual new spines has not been quantitatively addressed.

α -Amino-3-hydroxy-5-methyl-4-isoxazolepropionate (AMPA) and *N*-methyl-D-aspartate (NMDA) receptors are colocalized at the postsynaptic membrane of most excitatory synapses (Bekkers and Stevens, 1989; Kharazia and Weinberg, 1999; Nusser, 2000). The relative fraction of AMPA and NMDA receptors changes during development. In the early postnatal cortex a large fraction of hippocampal synapses contain mostly NMDA receptors (“silent synapses”), whereas more mature synapses are dominated by AMPA receptors. Silent synapses can accumulate AMPA-type glutamate receptors in an activity-dependent manner (Durand et al., 1996; Isaac et al., 1995; Liao et al., 1995, 1999; Petralia et al., 1999), a signature of synapse maturation. However, other studies suggest that AMPA and NMDA receptors arrive at hippocampal synapses at approximately the same time (Friedman et al., 2000; Hall and Ghosh, 2008; Xiao et al., 2004). It is therefore unclear if AMPA receptor insertion into silent synapses, or the formation of new synapses

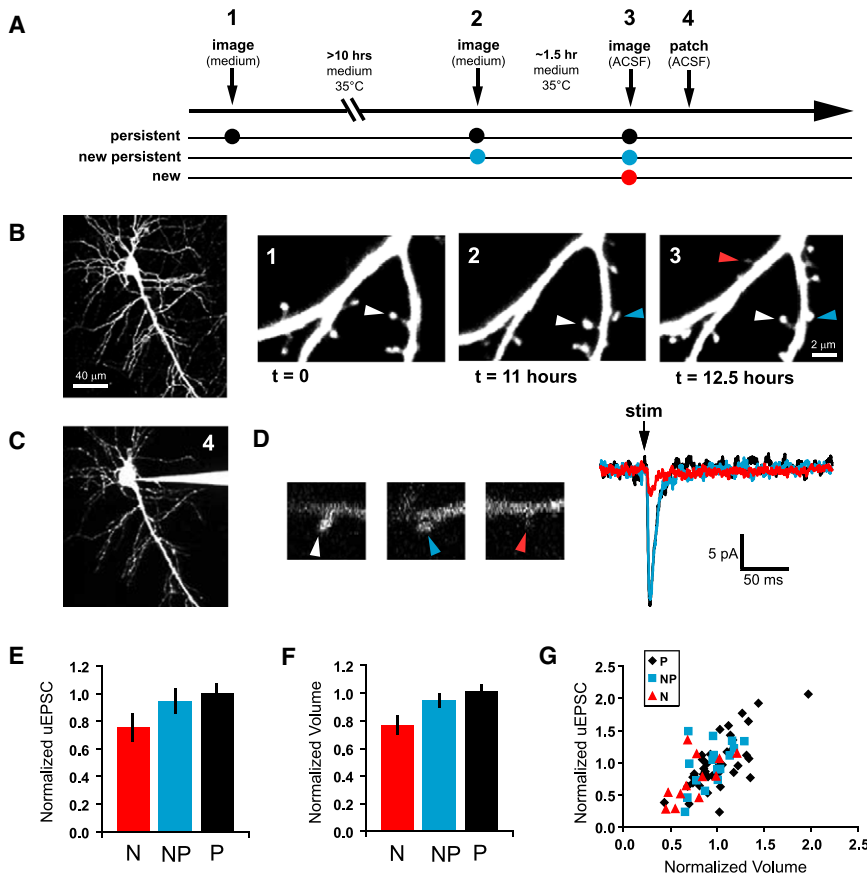


Figure 1. AMPA Receptor-Mediated Currents Are Comparable between New and Neighboring Persistent Spines

(A) Hippocampal pyramidal neurons in cultured brain slices were transfected with EGFP at 3 DIV. After 3–5 days, transfected slices were transferred to a chronic imaging chamber and imaged with a custom two-photon microscope. By imaging each dendrite three times (time points 1, 2, and 3 on timeline), we were able to classify spines into three age groups: persistent (black dots, >10 hr), new persistent (blue dots, ~2–12 hr), and new (red dot, <2.5 hr). After the final imaging session, we patched the imaged cell (time point 4 on timeline) and measured current responses to two-photon glutamate uncaging at individual new spines and their neighbors.

(B) A typical EGFP-transfected hippocampal pyramidal neuron (PND6 + 7 DIV). Dendrites were imaged the first and second times in medium ($t = 0$ and $t = 11$ hr), and a third time in ACSF ($t = 12.5$ hr). Arrowheads identify examples of spines from each age group: persistent (white arrowhead), new persistent (blue arrowhead), and new (red arrowhead).

(C) After the final time point, the imaged cell was patched, and whole-cell currents were recorded at -70 mV in ACSF containing (in mM): 1 Mg^{2+} , 2 Ca^{2+} , and 0.01 CPP, and 2.5 MNI-caged-L-glutamate.

(D) Current recordings from the persistent (black trace), new persistent (blue trace), and new (red trace) spines identified in (B), in response to glutamate uncaging at the site of the arrowheads. Traces are averages of five to seven trials. Vertical black arrow (“stim”) marks the time of the stimulus.

(E) AMPA current amplitudes (mean and standard error of the mean [\pm SEM]) from new (N; $n = 12$), new persistent (NP; $n = 16$), and persistent (P; $n = 37$) spines, normalized to the mean of all (≥ 4) P and NP currents from the same dendrite ($N = 9$ cells). AMPA current amplitudes of new spines are significantly smaller than those of persistent and new persistent spines ($p < 0.05$).

(F) As a measure of relative spine volume, peak fluorescence intensity for each spine was normalized to the mean peak fluorescence intensity of all (≥ 4) P and NP spines from the same dendrite. New spines are significantly smaller than persistent and new persistent spines (mean \pm SEM; $p < 0.01$).

(G) Normalized AMPA current amplitudes plotted against normalized volumes for persistent (black diamonds), new persistent (blue squares), and new (red triangles) spines. AMPA current amplitudes and spine volumes of persistent spines are highly correlated ($r = 0.72$; $p < 0.01$; $n = 37$). Data from new spines are similarly correlated ($r = 0.62$; $p < 0.05$; $n = 12$).

with AMPA receptors, accounts for the switch between silent and mature synapses.

How quickly do functional glutamate receptors accumulate on new spines? Do AMPA receptors arrive rapidly or after a prolonged delay following new spine formation? How does the arrival of glutamate receptors relate to the formation of anatomically mature synapses? To begin to address these questions, we examined the temporal relationship between spine growth and the accumulation of functional glutamate receptors. We used time-lapse two-photon microscopy of green fluorescent protein (GFP)-expressing hippocampal pyramidal neurons to identify spines of different ages, and then we characterized their functional properties using two-photon glutamate uncaging and electrophysiological measurements. We found that new spines were rapidly competent to respond to glutamate; AMPA receptor-mediated glutamate responses increased with spine age in lock-step with spine volumes. NMDA currents also developed rapidly, although calcium transient amplitudes were lower in new spines. Finally, we found that within a few hours of

outgrowth, new spines can participate in ultrastructurally mature synapses.

RESULTS

New Spines Have AMPA Receptors

To define the temporal relationship between spine growth and synapse formation, we used time-lapse two-photon microscopy to identify spines of different ages and then characterized their functional properties using two-photon glutamate uncaging and electrophysiological recording. Hippocampal pyramidal neurons in organotypic slice cultures from neonatal rat were transfected at 3–5 days in vitro (DIV) with GFP and imaged using a custom two-photon laser-scanning microscope. Dendrites of GFP-expressing neurons were imaged across multiple time points. By imaging each dendrite three times, we were able to classify spines into three age groups: persistent (>10 hr), new persistent (2–12 hr), and new (<2.5 hr; Figures 1A and 1B). Between image acquisitions, cells were maintained in culture

medium at 35°C. By imaging four dendritic segments per neuron (~200 μm total dendritic length), we consistently identified one to three new spines per cell.

Following the final imaging session, we patched the imaged cell and recorded excitatory postsynaptic currents evoked by two-photon photolysis of 4-methoxy-7-nitroindolyl (MNI)-caged glutamate (Matsuzaki et al., 2001; Sobczyk et al., 2005) at nascent spines and their neighbors (Figures 1C and 1D). We limited our analysis to spines that were within 160 μm of the soma, well separated (>1 μm) from other spines, and on dendritic segments that were oriented parallel to the surface of the slice. AMPA receptor-mediated whole-cell currents were recorded at -70 mV in the presence of an NMDA receptor blocker (CPP, 5 μM). Uncaging power (60–100 mW in the back focal plane [BFP]) was set to elicit a current of 10–15 pA from a control persistent spine, and then held constant for other spines on the same dendritic segment. The kinetics of uncaging-evoked excitatory currents (uEPSCs) closely matched those of spontaneous miniature EPSCs recorded from the same cell (Sobczyk et al., 2005) (Figure S1, available online).

uEPSC amplitudes ranged from 2 to 21 pA for persistent spines ($n = 37$), 1 to 17 pA for new persistent spines ($n = 16$), and 2 to 13 pA for new spines ($n = 12$; Figure S2A). Because of a broad range of depths in the brain slices (~20–60 μm) and the heterogeneous milieu in the tissue surrounding GFP-transfected cells, the efficiency of glutamate uncaging differed for dendrites recorded in different preparations. Therefore, to compare data across multiple cells recorded in different brain slices, we normalized uEPSC amplitudes from each spine to the average uEPSC amplitude of all persistent and new persistent spines on the same dendrite. Normalized uEPSC amplitudes of persistent (1.02 ± 0.07) and new persistent (0.95 ± 0.09) spines were not significantly different ($p > 0.5$; Figure 1E). In contrast, new spines had significantly smaller normalized uEPSC amplitudes (0.75 ± 0.1) than those of persistent and new persistent spines ($p < 0.05$; Figure 1E).

We estimated the currents contributed by AMPA receptors on dendritic shafts (including possible shaft synapses) by uncaging at similar distances from the shaft as before, but now in the absence of a spine. Normalized uEPSC amplitudes of new spines (0.75 ± 0.1) were significantly larger than those of dendrites (0.22 ± 0.05 ; $p < 0.001$; $n = 8$; Figure S3A). For a subset of spines (3 persistent, 2 new persistent, and 3 new), uEPSC amplitudes were within 2 standard deviations (SD) of the expected dendritic currents; these spines could lack AMPA receptor clusters. Yet rise times (stimulus to peak) for all but 3 (1 persistent, 1 new persistent, and 1 new) of these 8 spines were within 2 SD (1.8 ms) of the mean rise time (3.8 ms) of persistent spines with significant uEPSC amplitudes, suggesting that most of these small responses arise from AMPA receptors on the spine.

Because earlier studies suggested that uEPSC amplitude is proportional to spine volume (Matsuzaki et al., 2001; Sobczyk et al., 2005), we wondered whether the smaller uEPSC amplitudes seen in new spines reflected smaller spine volumes. We used brightness as a measure of relative spine volume (Nimchinsky et al., 2004). Brightness values (maximum pixel intensities) for each spine were normalized to the mean value for all persis-

tent and new persistent spines on the same dendrite. Normalized volumes of new spines (0.77 ± 0.07) were significantly smaller than those of persistent (1.03 ± 0.05) and new persistent (0.94 ± 0.07) spines ($p < 0.01$; Figure 1F). By plotting normalized uEPSC amplitudes against normalized volumes, we indeed observed that new spines respond to glutamate at levels comparable to persistent spines of similar volumes (Figure 1G).

To determine the time course of functional spine maturation, we performed acute imaging experiments in which dendrites of GFP-transfected hippocampal pyramidal neurons were imaged every 10–12 min at 35°C until a new spine formed (Figure 2A). Immediately after the final time point, we patched the imaged cell and measured uEPSCs at new spines and their neighbors (Figure 2B). uEPSC amplitudes ranged from 2 to 9 pA for these “early” new spines ($n = 8$) and 1 to 18 pA ($n = 31$) for neighboring control spines (Figure S2B). Normalized uEPSC amplitudes of early new spines (0.68 ± 0.19) were smaller than those of control spines (1.0 ± 0.10 ; $p < 0.1$; one-tailed *t* test; Figure 2C). Consistent with the hypothesis that smaller response amplitudes of early new spines are correlated with smaller spine size, we found that new spines had correspondingly smaller normalized volumes (0.62 ± 0.13) than control spines (1.00 ± 0.08 ; $p < 0.05$). By plotting normalized uEPSC amplitudes against normalized volume, we observed that even very young new spines respond to glutamate at levels comparable to persistent spines of similar volumes (Figure 2D).

Normalized uEPSC amplitudes of early new spines (0.68 ± 0.19) were significantly larger than those of dendrites (0.25 ± 0.10 ; $p < 0.05$; $n = 6$; Figure S3B); however, for a subset of spines (13 control and 4 new), uEPSC amplitudes were within 2 SD of the expected dendritic currents. Rise times (stimulus to peak) for all but 3 (2 control and 1 new) of these 17 spines were within 2 SD (2.4 ms) of the mean rise time (4.7 ms) for control spines with significant uEPSC amplitudes, suggesting that most of these small responses arise from AMPA receptors on spines.

We estimated spine age as half of the interval between the time point at which the spine was first observed and the time point immediately prior. The median age of new spines was 35 min in the acute imaging experiments and 1.8 hr in the chronic imaging experiments. As spine age increased, spines grew in volume, and AMPA receptor current amplitudes increased (Figure 2E). The proportional relationship between spine volume and AMPA current amplitudes is retained across spines of all age categories ($p > 0.4$ for all pairwise relationships; Figure 2F). We found no evidence that spine outgrowth and the accumulation of AMPA receptors were separated in time by more than a few tens of minutes (Figures 1G and 2D).

Our data are consistent with a model whereby functional AMPA receptors accumulate rapidly in new spines as spine size increases. In addition to synaptic glutamate receptors in the postsynaptic density, the spine membrane likely contains a lower density of extrasynaptic receptors (Figure 2G). What are the contributions of these extrasynaptic receptors to uEPSCs? Assuming a uniform distribution of extrasynaptic receptors, we calculated the relationship between the number of activated receptors and spine head volume for situations with different fractions of synaptic and extrasynaptic receptors (Supplemental Experimental Procedures). Our data are consistent with synaptic

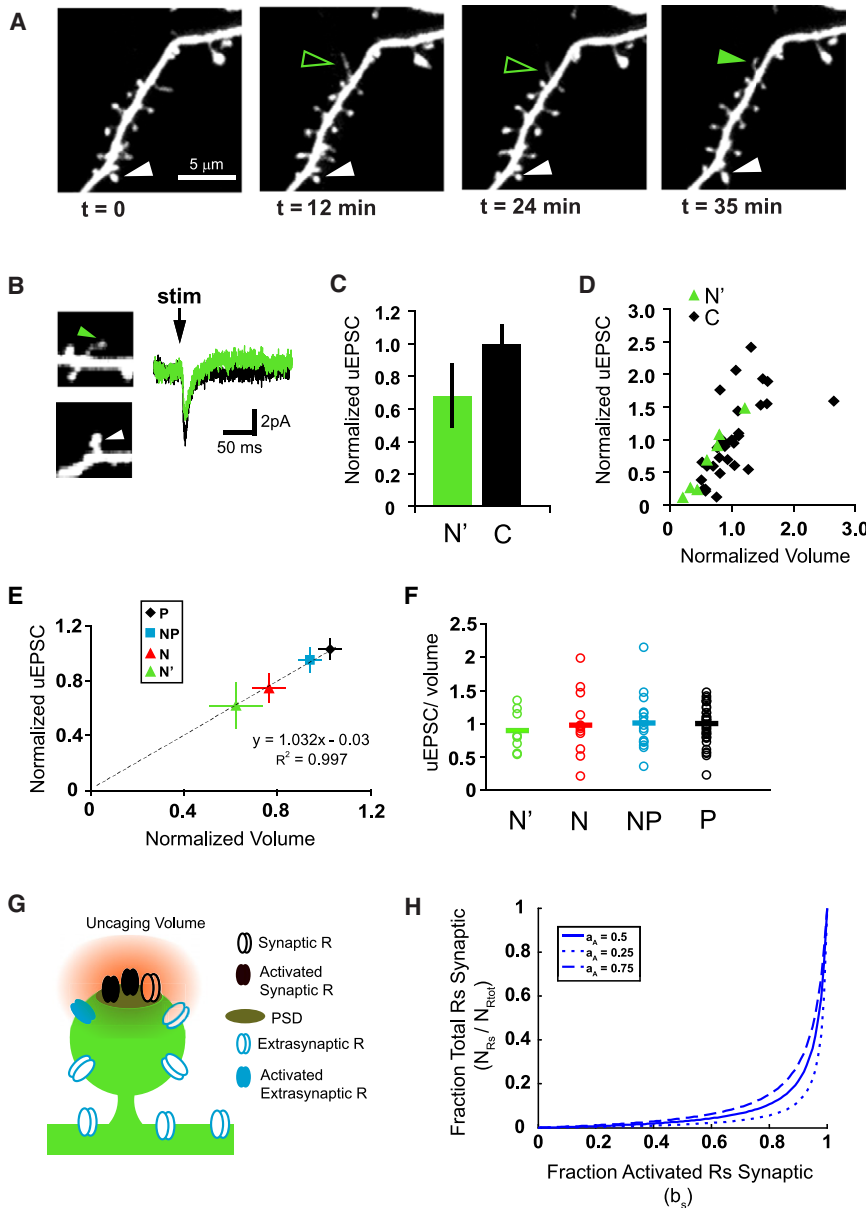


Figure 2. AMPA Receptor-Mediated Currents of Developing Spines Mature Coincident with Increase in Spine Volume

(A) Dendrites of GFP-transfected hippocampal pyramidal neurons were imaged every 10–12 min in ACSF at 35°C. Spines were classified into two groups: control (C; present at all time points; e.g., white arrowhead), and early new (N'; appearing after the first time point; e.g., green arrowhead). Early new spines were all less than 50 min old.

(B) After time-lapse imaging, the cells were patched and whole-cell currents were recorded at the soma. Shown are current recordings in response to glutamate uncaging at the control (black trace) and early new (green trace) spines identified in (A). Each trace is the average of five to seven trials. Vertical black arrow (stim) marks the time of the stimulus.

(C) AMPA current amplitudes (mean \pm SEM) from early new (N'; n = 7) and control (C; n = 31) spines normalized to the mean of all (≥ 3) C currents from the same dendrite (N = 7 cells). AMPA current amplitudes of early new spines are smaller than those of control spines ($p < 0.1$; one-tailed t test).

(D) Normalized AMPA current amplitudes plotted against normalized volumes for control (C; black diamonds), and early new (N'; green triangles) spines. AMPA current amplitudes and spine volumes of control spines are highly correlated ($r = 0.65$; $p < 0.01$; 31 control spines). Data from early new spines appear similarly correlated ($r = 0.98$; $p < 0.01$; n = 7).

(E) Mean normalized AMPA current amplitudes plotted against mean normalized volumes for early new (N'; green triangle), new (N; red triangle), new persistent (NP; blue square), and persistent (P; black diamond) spines. Across developmental time, mean AMPA current amplitudes increase linearly with increase in spine volume ($R^2 = 0.999$). Error bars represent SEM.

(F) Summary of normalized AMPA current amplitude to volume relationships for individual early new (N'; n = 8), new (N; n = 12), new persistent (NP; n = 15), and persistent (P; n = 37) spines. Horizontal bars represent mean values.

(G) Schematic of the experimental configuration, showing the activation of synaptic and extrasynaptic receptors that are within the cloud of uncaged glutamate. The intersection of this cloud with the spine head defines the photoactivated spine head area (a_A).

(H) Fraction of total receptors that are synaptic versus the fractional contribution of synaptic receptors to the uEPSC (Experimental Procedures, Equation 4). Plots correspond to different values for the fraction of the photoactivated spine head area ($a_A = 0.25$, dotted line; $a_A = 0.5$, continuous line; $a_A = 0.75$, broken line). The fraction of the total surface area on spines, $R_{SH/total} = 0.0595$, was derived from EM reconstructions (see Figure 5). If synaptic receptors contribute less than 80% to the uEPSC ($b_s < 0.8$), then less than 10% of all receptors would be synaptic ($N_{RS}/N_{Rtot} < 0.1$).

receptors providing most of the response. Based on reconstructed dendritic segments from SSEM (see Figure 5), we further estimated the fraction of total receptors that would have to be extrasynaptic to produce substantial responses when stimulating spines (Experimental Procedures). These calculations show that if extrasynaptic receptors contributed substantially ($>20\%$) to uEPSCs, then the vast majority ($>80\%$) of receptors would have to be extrasynaptic (Figure 2H). This contradicts AMPA receptor distributions measured with immuno-electron

microscopy (e.g., Baude et al., 1995; Kharazia and Weinberg, 1999; Nusser et al., 1998). We conclude that new spines contain synaptic glutamate receptors.

NMDA Receptor-Mediated Ca^{2+} Signals in New Spines

We next probed the relationship between spine growth and the accumulation of NMDA receptors. As before, we used time-lapse two-photon microscopy to identify spines of different ages (Figure 3A) and then measured their NMDA receptor-mediated

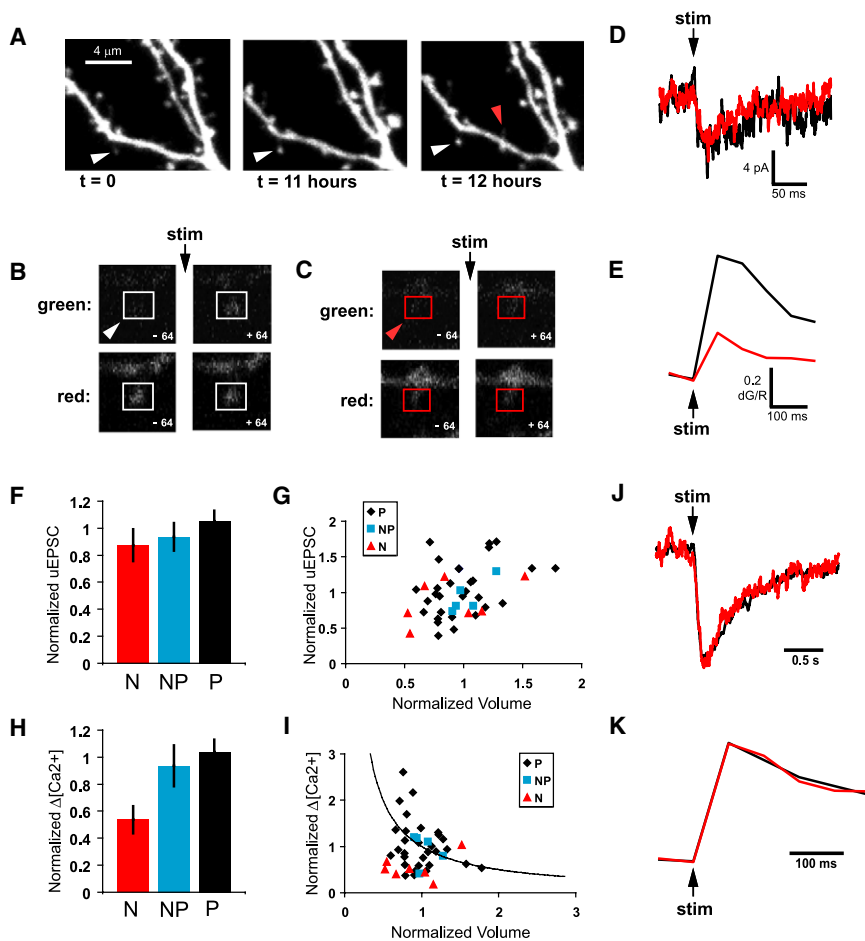


Figure 3. NMDA Receptor-Mediated $[Ca^{2+}]$ Transients Are Lower in New Spines

(A) Dendrites of GFP-transfected hippocampal pyramidal neurons were imaged three times. Spines were classified into three age groups: persistent (>10 hr), new persistent (~ 2 – 10 hr), and new (<2 hr). Arrowheads identify examples of persistent (white) and new (red) spines.

(B–E) After the final time point, the imaged cell was patched and filled with 0.03 mM Alexa-594 (red; Ca^{2+} -insensitive signal) and 1 mM Fluo-5F (green; Ca^{2+} -sensitive signal). Whole-cell currents and calcium responses were recorded at -70 mV in ACSF containing (in mM): 0.1 Mg^{2+} , 3 Ca^{2+} , and 0.01 NBQX, 0.01 d-serine, 0.02 ryanodine, 0.001 thapsigargin, and 2.5 MNI-caged-L-glutamate. Each trial consisted of a series of sequential frames of 64 ms. Boxes were drawn surrounding the region of interest (ROI) containing the spine head for the persistent [(B), white boxes] and new [(C), red boxes] spines identified in (A). Calcium transient amplitude was calculated as the ratio of the change in Ca^{2+} -sensitive green signal over the Ca^{2+} -insensitive red signal (dG/R), and calcium transient amplitude was measured as the signal in the first poststimulus frame minus the mean signal of two baseline frames. Shown are current (D) and calcium (E) recordings in response to glutamate uncaging at the persistent (black) and new (red) spines identified in (A). Traces are averages of five to seven trials. Vertical black arrow (stim) marks the time of the stimulus.

(F) NMDA current amplitudes (mean \pm SEM) from new (N; $n = 7$), new persistent (NP; $n = 5$), and persistent (P; $n = 25$) spines normalized to the mean of all (≥ 4) P and NP currents from the same dendrite. There is no significant difference between NMDA current amplitudes of new spines and those of persistent and new persistent spines ($p > 0.3$).

(G) Normalized NMDA current amplitudes plotted against normalized volumes for persistent (black diamonds), new persistent (blue squares), and new (red triangles) spines. NMDA current amplitudes are only weakly correlated with spine volumes ($r = 0.38$; $p < 0.05$; 30 persistent and new persistent spines).

(H) Normalized $[Ca^{2+}]$ transient amplitudes (mean \pm SEM) from new (N; $n = 7$), new persistent (NP; $n = 5$), and persistent (P; $n = 25$) spines, recorded simultaneously with NMDA currents (A) and (B) from the same seven cells. Data are normalized to the mean of all (≥ 4) P and NP $[Ca^{2+}]$ transient amplitudes from the same dendrite. $[Ca^{2+}]$ transient amplitudes of new spines are significantly lower than those of persistent and new persistent spines ($p < 0.05$).

(I) Normalized $[Ca^{2+}]$ transient amplitudes plotted against normalized volumes for persistent (black diamonds), new persistent (blue squares), and new (red triangles) spines. The black curve represents the function $1/(\text{spine volume})$. Independent of spine volume, $[Ca^{2+}]$ transient amplitudes of new spines are consistently lower than those of mature spines.

(J) Average uEPSC from new (red) and persistent (black) spines, normalized to peak amplitude. Vertical black arrow (stim) marks the time of the stimulus. Kinetics of NMDA currents are comparable in new and persistent spines.

(K) Average $[Ca^{2+}]$ transient from new (red) and persistent (black) spines, normalized to peak amplitude. Vertical black arrow (stim) marks the time of the stimulus. Kinetics of $[Ca^{2+}]$ transients are comparable in new and persistent spines.

responses using two-photon glutamate uncaging combined with simultaneous calcium imaging and electrophysiological recording (Figures 3B–3E).

Immediately after time-lapse imaging, neurons were patched and loaded with Ca^{2+} -sensitive (green, Fluo-5F; Figures 3B and 3C, top row) and Ca^{2+} -insensitive (red, Alexa 594; Figures 3B and 3C, bottom row) fluorophores. To ensure a linear relationship of $[Ca^{2+}]$ and fluorescence while minimizing saturation of the calcium indicator, we used a high concentration (1 mM) of the medium-affinity ($K_D \sim 1.6 \mu\text{M}$) indicator Fluo-5F (Sabatini et al., 2002; Sobczyk et al., 2005; Yasuda et al., 2004). NMDA receptor-mediated whole-cell currents (Figure 3D) and calcium

transients (Figure 3E) were recorded in low extracellular Mg^{2+} (0.1 mM) at -70 mV, and in the presence of drugs that block AMPA receptors (NBQX, 10 μM) and calcium release from internal stores (20 μM ryanodine and 1 μM thapsigargin). We used focal photolysis of MNI-glutamate to stimulate individual spines. Uncaging power (60–100 mW in the BFP) was set to elicit currents of 5–8 pA from a control persistent spine, and then held constant for the remainder of that dendritic segment. The amplitude of $[Ca^{2+}]$ transients (dG/R ; Figure 3E) was calculated as the change in green fluorescence (ΔG) normalized by the red fluorescence (R) within regions of interest containing the spine head (Figures 3B and 3C).

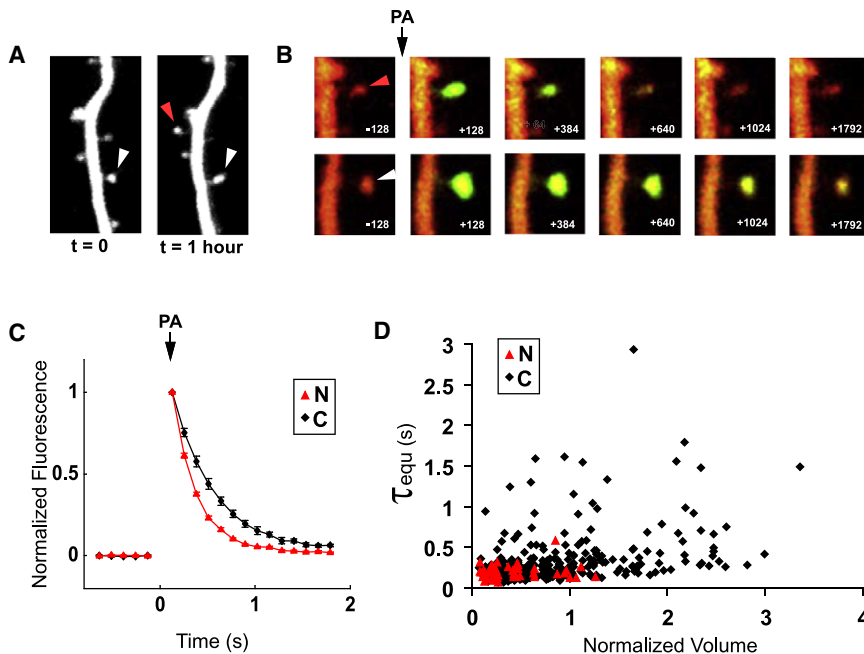


Figure 4. New Spines Are More Tightly Coupled to the Dendrite

(A) Dendrites of hippocampal pyramidal neurons cotransfected with dsRedExpress and paGFP were imaged the first in medium ($t = 0$ hr) and then in ACSF ($t = 1$ hr). Shown are the images from the red channel (dsRedExpress). Spines were classified into two groups: new (appearing in the second time point; e.g., red arrowhead) and control (present at both time points; e.g., white arrowhead).

(B) Images collected before and after photoactivation ("PA") for the new (red arrowhead; top row) and control (white arrowhead; bottom row) spines from (A), showing overlay of dsRedExpress (red) and paGFP (green) fluorescence. Overlap of green and red fluorescence appears yellow. Time stamps are in milliseconds.

(C) Time course of paGFP fluorescence decay after photoactivation (PA) for the new (N; red triangles) and control (C; black diamonds) spines from (A and B). The data points following photoactivation were fit to a single exponential to extract the time constant of equilibration (τ_{equ}). Error bars represent SEM.

(D) τ_{equ} plotted against normalized volumes for new (N; red triangles; $n = 47$) and control (C; black diamonds; $n = 321$) spines from 36 cells. For all spines of normalized volumes 1.5 or less, only 2% of new spines had τ_{equ} greater than 350 ms, as compared with 18% of control spines.

NMDA current amplitudes ranged from 2 to 17 pA for persistent spines ($n = 25$), 4 to 6 pA for new persistent spines ($n = 5$), and 2 to 8 pA for new spines ($n = 7$; Figure S2C). There was no significant difference between normalized NMDA current amplitudes of persistent (1.04 ± 0.07), new persistent (0.94 ± 0.1), and new (0.87 ± 0.1) spines ($p > 0.25$; Figure 3F). Normalized uEPSC amplitudes from new spines were significantly larger than those of dendrites (0.26 ± 0.08 ; $p < 0.001$; $n = 5$; Figure S3C). However, for a small subset of spines (2 persistent and 1 new), uEPSC amplitudes were within 2 SD of the expected dendritic currents; these spines could lack NMDA receptor clusters. Our data confirm previous reports that NMDA-receptor-mediated current amplitudes are relatively constant across spines of different volumes (Noguchi et al., 2005; Sobczyk et al., 2005) (Figure 3G). We conclude that NMDA currents of new spines are comparable to those of persistent spines. Furthermore, like AMPA receptors, NMDA receptors accumulate rapidly at nascent spines.

Despite having similar NMDA currents, new spines had significantly smaller normalized calcium transient amplitudes (0.54 ± 0.10) than neighboring persistent (1.04 ± 0.12) and new persistent (0.94 ± 0.15) spines ($p < 0.05$; Figure 3H). This result was not a consequence of differences in spine volumes, because new spines consistently exhibited smaller calcium transients across all spine volumes (Figure 3I). Indeed, although spines display a large variability in the amount of calcium influx per unit current ($\Delta[\text{Ca}^{2+}]/\text{uEPSC}$) (Sobczyk et al., 2005), new spines showed a significantly lower calcium to current ratio (0.13 ± 0.03) than persistent (0.22 ± 0.03) spines ($p < 0.05$). We hypothesized that new spines might contain NMDA receptors of different subunit compositions, which exhibit different deactiva-

tion kinetics (Liu et al., 2004; Tovar and Westbrook, 1999); shorter currents mean smaller $\Delta[\text{Ca}^{2+}]$ for the same current amplitude. However, we found no substantial difference in the kinetics of NMDA currents (Figure 3J) or calcium transients (Figure 3K) in new versus persistent spines.

Our measurements imply that $[\text{Ca}^{2+}]$ handling is immature in new spines. In our experiments the presence of high concentrations (1 mM) of medium-affinity Ca^{2+} indicator ($K_d \sim 1.6 \mu\text{M}$ for Fluo-5F) dominates intracellular buffers (Sabatini et al., 2002) and greatly prolongs cytoplasmic Ca^{2+} transients. Under these conditions, diffusion of indicator-bound Ca^{2+} from the spine head to the parent dendrite is likely a major mode of decay of Ca^{2+} accumulations in the spine head. Therefore, we directly measured diffusional coupling between spine heads and their parent dendrites (Bloodgood and Sabatini, 2005; Noguchi et al., 2005; Sobczyk et al., 2005; Svoboda et al., 1996) in new spines and their neighbors using neurons transfected with the photoactivatable green fluorophore, paGFP (Patterson and Lippincott-Schwartz, 2002). Photoactivation of paGFP within individual spines triggers increases in fluorescence within the spine head that dissipates as activated paGFP diffuses into the dendrite (Bloodgood and Sabatini, 2005). The decay of fluorescence transients in the spine head is well fit by a single exponential, yielding a time constant of equilibration (Svoboda et al., 1996), τ_{equ} , of paGFP across the spine neck (Bloodgood and Sabatini, 2005). Spines with stronger diffusional coupling (shorter τ_{equ}) are expected to have smaller $\Delta[\text{Ca}^{2+}]/\text{uEPSC}$ (Sobczyk et al., 2005).

Dendrites of hippocampal pyramidal neurons cotransfected with dsRedExpress and paGFP were imaged at 1 hr intervals to identify new spines (Figure 4A). Immediately after the second

time point, we measured fluorescence decay after photoactivation of paGFP at new spines and their neighbors (Figures 4B and 4C). τ_{equ} values ranged from 0.06 to 0.59 s for new ($n = 47$) and 0.07 to 2.93 s for neighboring control ($n = 321$) spines. New spines had significantly smaller τ_{equ} values (0.19 ± 0.01 s) than those of control (0.31 ± 0.02 s) spines ($p < 0.05$). The smaller τ_{equ} values of new spines could in part be attributed to the reduced size of new (0.48 ± 0.06) versus control (1.0 ± 0.04) spines ($p < 0.001$). Plotting τ_{equ} against normalized volume revealed that τ_{equ} values for new spines are consistently at the lower end of the range, irrespective of spine volume (Figure 4D). Thus, smaller $\Delta[\text{Ca}^{2+}]_{\text{uEPSC}}$ in new spines might be at least partially attributable to stronger diffusional coupling between new spines and the dendrite.

New Spines Make Synapses

New dendritic spines contain postsynaptic glutamate receptors within a few hours of outgrowth, but do these spines contact presynaptic elements? To address this question, we performed SSEM and 3D reconstructions on dendrites from two cells that had been previously imaged and electrophysiologically characterized (Figures 5 and S5).

New spines (<2.5 hr) were identified by time-lapse imaging (Figures 5A and S5A) and uEPSCs were recorded from individual spines in response to two-photon glutamate uncaging (Figure 5B). Immediately after whole-cell recording, cells were fixed for SSEM. Previously imaged dendrites were readily identified by immunostaining for GFP (Figures S6 and S7). Each of the three reconstructed new spines showed all of the hallmarks of synapses (Colonnier, 1968): they had a clear a synaptic cleft, and a postsynaptic density apposed to a presynaptic bouton containing synaptic vesicles (Figures 5C, 5D, S5B, and S5C). We did not find obvious ultrastructural differences (postsynaptic density area, spine neck width, volume of contacting presynaptic bouton) between the new spines and their neighbors (Table S1). We conclude that synapse formation onto dendritic spines can occur rapidly, within a few hours of spine outgrowth.

DISCUSSION

Glutamate Receptor Content of New Spines

We measured the glutamate receptor content of new spines. We found that, within a few hours after spine growth, both AMPA- and NMDA-type glutamate receptor currents are indistinguishable from those of mature spines of similar volumes. Even in the youngest spines probed (median age 35 min), AMPA currents were not distinguishable from older spines when corrected for differences in spine volume. We did not find evidence for a separate category of new spines with substantial spine volumes and small current amplitudes, a category that would be predicted if spine outgrowth preceded glutamate receptor accumulation with a long (>30 min) time delay. Quantitative modeling based on electron microscopy (EM) reconstructions suggests that extrasynaptic receptors played a negligible role in spine responses. Instead, our results support a model in which postsynaptic receptor content of new spines develops essentially concurrent with spine growth. Such a model is consistent with tight coupling between the delivery of AMPA-type glutamate receptors, insertion of

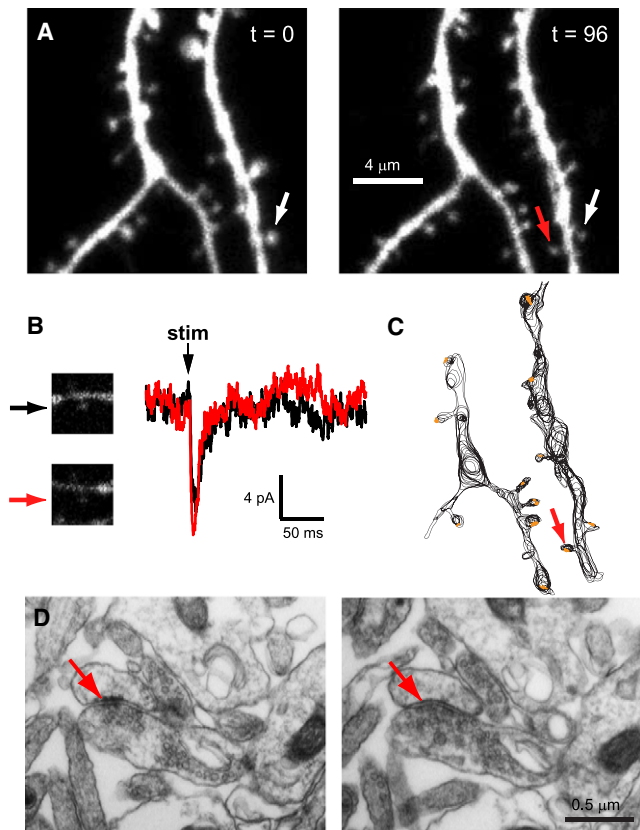


Figure 5. Ultrastructural Evidence for Synapses on New Spines

(A) A new spine (red arrow) appeared across from a persistent spine (white arrow) during time-lapse imaging of dendrites from a GFP-transfected hippocampal pyramidal neuron. The two time points were separated by 96 min in medium at 35°C. (B) After time-lapse imaging, the cell was patched and whole-cell currents were recorded at the soma. Shown are current recordings from the persistent (black trace) and new (red trace) spines identified in (A), in response to glutamate uncaging at each individual spine (arrows). Each trace is the average of five to seven trials. Vertical black arrow (stim) marks the time of the stimulus. (C) NeuroLucida drawing of reconstructed dendrites from (A). After imaging and current recordings, the cell was immediately fixed and stained for GFP. Black lines show the contours of the labeled dendrite and spines from consecutive images taken from serial thin sections in the electron microscope. Synapses are shown in orange. The red arrow identifies the new spine (age between 118 and 214 min at the time of fixation) from (A) and (B). (D) Electron micrographs from two consecutive serial sections through the new spine (same as indicated by red arrows in [A]–[C]). The red arrow points to a dense region of staining within the spine, which is apposed to an axonal bouton containing vesicles.

membrane lipids, and spine enlargement (Kopeck et al., 2007; Matsuzaki et al., 2004; Park et al., 2006).

Our observation that AMPA currents develop rapidly in new spines does not exclude the possibility of “silent” synapses, proposed to contain only NMDA receptors (Beique et al., 2006; Busetto et al., 2008; Durand et al., 1996; Isaac et al., 1996; Liao et al., 1995; Petralia et al., 1999; Wu et al., 1996). Consistent with previous experiments (Matsuzaki et al., 2001) we find that the expression level of functional AMPA receptors in spines is strongly correlated with spine volume, whereas functional

NMDA receptor levels and spine volumes are only weakly correlated (Noguchi et al., 2005; Sobczyk et al., 2005). Because AMPA receptor content increases much more rapidly with spine volume than NMDA receptor content, smaller spines exhibit lower AMPA to NMDA ratios (Matsuzaki et al., 2004; Racca et al., 2000; Takumi et al., 1999). In fact, a small subset of our spines, primarily those with smallest volumes, exhibited responses indistinguishable from noise. However, these potentially silent spines were found in all spine age categories, neither restricted to nor biased toward new spines. We would predict that if all new spines are indeed initially silent, then in most cases this phase would be very short-lived, at least during the postnatal periods of our study.

[Ca²⁺] Handling in New Spines

Although NMDA receptor currents were indistinguishable between new and mature spines, Ca²⁺ transients mediated by NMDA receptors were significantly lower in new spines. This surprising result was not a consequence of differences in spine volumes, because new spines consistently exhibited smaller calcium transients across all spine volumes. Multiple factors determine [Ca²⁺] transient amplitude in spine heads: (1) magnitude of Ca²⁺ influx, (2) spine volume, (3) Ca²⁺ buffer capacity, (4) extrusion of Ca²⁺, and (5) diffusional coupling between the spine head and its parent dendrite. Under our experimental conditions the Ca²⁺ indicator dominated intracellular buffers and slowed extrusion of Ca²⁺ by more than 20-fold (Yasuda et al., 2004). Diffusional coupling between spine head and dendrite is therefore likely a major factor shaping the [Ca²⁺] transient amplitude. Indeed, we found that new spines exhibited stronger diffusional coupling with the dendrite. These differences could partially explain lower calcium accumulations in new spines.

Differences in Ca²⁺ influx also likely contribute to differences in Ca²⁺ signals in new and mature spines. New spines might have different NMDA receptor subunit compositions than control spines, and spine maturation might be accompanied by rapid exchange of NMDA receptor subunit types (Bellone and Nicoll, 2007). However, we did not observe substantial differences in NMDA current decay kinetics, although such differences can be small (Sobczyk et al., 2005) and therefore difficult to measure at the level of single spines. Alternatively, new spines might contain NMDA receptors with lower Ca²⁺ permeabilities due to different phosphorylation states (Skeberdis et al., 2006), and therefore exhibit lower calcium influx for the same current amplitude (Skeberdis et al., 2006; Sobczyk et al., 2005; Sobczyk and Svoboda, 2007). These differences in Ca²⁺ signaling could differentiate the induction threshold for long-term potentiation and long-term depression in new versus old spines. We would predict that new spines would be harder to potentiate, and possibly to stabilize (Lohmann et al., 2005), compared with older spines. This could ensure that only the most favorable new synapses become stabilized.

Relationship between Spine Growth and Synapse Formation

Our experiments provide new insights into the time course of synapse assembly on nascent spines. We provide evidence that spine synapses can form rapidly, within hours of new spine growth. Our measurements have much higher time resolution

than previously reconstructed new spine synapses from in vivo imaging experiments (imaged at intervals of 1–4 days; (Holtmaat et al., 2006; Knott et al., 2006; Trachtenberg et al., 2002). Those studies suggested that in vivo, new spines make synapses over a prolonged time, probably exceeding 1 day (Knott et al., 2006). Timing differences between the two studies are most likely explained by differences in the dynamics of synapse formation in the adult brain in vivo compared with developing neurons in vitro. Although we cannot definitively rule out that the synapses we observed were in fact already present on the dendrite before spine growth, we think it is unlikely based upon previous studies that demonstrated that spine outgrowth preceded accumulation of postsynaptic markers by at least 20 min (De Roo et al., 2008; Okabe et al., 2001).

Our results demonstrating rapid synapse formation onto a subset of new spines are in agreement with data from dissociated cultured neurons, which suggest rapid synapse assembly after contact between pre- and postsynaptic elements (Buchanan et al., 1989; Friedman et al., 2000; Okabe et al., 2001; Washbourne et al., 2002; Ziv and Smith, 1996). Our results are in contrast with those from a recent study (Nagerl et al., 2007), in which new spines of hippocampal pyramidal neurons in slice culture were characterized using EM at different times after spine outgrowth. In those experiments synapse formation onto new spines did not occur until 15–19 hr after spine outgrowth. The discrepancy between the two studies is most likely a consequence of differences in experimental design (Supplemental Discussion). Most notably, our data are from spines that grew spontaneously; in contrast, Nagerl and colleagues focused on new spine outgrowth in response to tetanic stimulation.

Do all new spines form synapses? Our data show that the majority of, or perhaps all, new spines rapidly accumulate glutamate receptors. Furthermore, we detected ultrastructurally mature synapses on a subset of new spines within a few hours of spine outgrowth. These observations suggest that the majority of new spines in fact participate in synaptic contacts at some point during their life cycle.

EXPERIMENTAL PROCEDURES

Hippocampal Slice Culture and Transfection

Hippocampal slices were prepared from P6 or P7 rats as described (Stoppini et al., 1991) in accordance with animal care and use guidelines of Cold Spring Harbor Laboratory. Genes were delivered at 3–5 DIV using particle-mediated biolistic gene transfer (180 psi), as described previously (Zito et al., 2004), except 15 μg pEGFP-N1 (Clontech) was coated onto 8 mg 1.6 μm gold beads.

Chronic and Acute Time-Lapse Imaging of New Spine Growth

GFP-transfected pyramidal neurons were imaged 3–5 days after transfection using a custom two-photon microscope with a pulsed Ti:sapphire laser (Mira, Coherent) tuned to 910 nm. For each neuron, two segments of secondary basal dendrites and two segments of secondary apical dendrites were imaged. For chronic time lapse, slices were returned to the incubator (35°C) between imaging sessions. The first two imaging sessions were in culture medium, and the final imaging session was in artificial cerebrospinal fluid (ACSF) consisting of (in mM): 127 NaCl, 25 NaHCO₃, 25 D-glucose, 2.5 KCl, and 1.25 NaH₂PO₄, 1 MgCl₂, 2 CaCl₂, aerated with 95% O₂/5% CO₂. For some experiments we substituted 0.1 mM MgCl₂ and 3 mM CaCl₂ (see figure legends). By imaging each dendrite three times, we were able to classify spines into three age groups: persistent (>10 hr), new persistent (~2–12 hr), and new (<2.5 hr). For acute time lapse, slices were imaged every

10–12 min at 35°C in ACSF containing 0.01 mM D-serine. Spines were classified into two age groups: early new (<1 hr) and control.

Electrophysiology and Glutamate Uncaging

Whole-cell voltage-clamp recordings (holding potential -70 mV) were obtained at 25°C directly after time-lapse imaging. Access resistances were 20–40 M Ω for chronic time-lapse experiments, and 30–95 M Ω for acute time-lapse experiments. Patch pipette (4–6 M Ω) internal solution consisted of (in mM): 120 CsMeSO₃, 20 CsCl, 10 HEPES, 4 Mg₂ATP, 0.3 Na₂GTP, 14 phosphocreatine, 4 NaCl, 3 ascorbate, 0.03 Alexa 594, 1 Fluo-5F (pH adjusted to 7.3 with CsOH). AMPA receptor-mediated current recordings were performed in ACSF containing (in mM): 1 MgCl₂, 2 CaCl₂, 0.001 TTX, 0.01 CPP, and 2.5 mM MNI-caged-L-glutamate.

NMDA receptor-mediated current recordings were performed in ACSF containing (in mM): 0.1 MgCl₂, 3 CaCl₂, 0.001 TTX, 0.01 2,3-dihydroxy-6-nitro-7-sulfonyl-benzof[*q*]quinoxaline (NBQX), 0.02 ryanodine, 0.001 thapsigargin, 0.01 D-serine, and 2.5 mM MNI-caged-L-glutamate. This mixture abolished calcium release from intracellular stores, as tested by application of caffeine (Garaschuk et al., 1997; Sobczyk et al., 2005). The small amplitudes of the NMDA receptor-mediated currents (<10 pA with two exceptions) ensured that activation of voltage-gated calcium channels did not occur (Sobczyk et al., 2005). TTX was obtained from Calbiochem, MNI-caged-L-glutamate from NBQX, thapsigargin from Tocris, Ca²⁺ indicators from Molecular Probes, and all other reagents from Sigma.

Individual dendritic spines were stimulated by focal photolysis of MNI-caged-L-glutamate while recording whole-cell uEPSCs at the soma, as described previously (Sobczyk et al., 2005). In brief, uncaging of MNI-caged-L-glutamate was accomplished by directing a pulsed Ti:sapphire laser (Mai Tai, Spectra Physics) tuned to 720 nm (60–100 mW in the objective BFP) for 0.25 ms at a standard uncaging location, ~ 0.5 μ m from the center of the spine head in the direction away from the parent dendrite. Beam intensity was controlled via an electro-optical modulator (Conoptics). Data acquisition and glutamate uncaging were controlled by ScanImage (Pologruto et al., 2003). Uncaging-evoked current (uEPSC) amplitudes were calculated as the mean amplitude after baseline subtraction (window: 3–5 ms after stimulus for AMPA currents [chronic experiments], 3.4–5.8 ms after stimulus for AMPA currents [acute experiments], and 6 ms around the peak for NMDA currents).

Calcium Imaging

Calcium imaging was performed simultaneous with glutamate uncaging and current recordings (Carter and Sabatini, 2004; Sobczyk et al., 2005) using a pulsed Ti:sapphire laser (Mira, Coherent) tuned to 810 nm; this wavelength efficiently excited the Ca²⁺ indicator, but not GFP. Calcium imaging (810 nm) and glutamate uncaging (720 nm) beams were combined with a polarizing beam splitting cube (CVI Laser Optics) and passed through the same set of scan mirrors and objective (60 \times , 0.9 NA, Olympus). Following break-in for whole-cell recordings, cells were loaded for 20 min with internal solution (see above) containing 1 mM Fluo5F (Ca²⁺ sensitive green signal [G]) and 0.03 mM Alexa 594 (Ca²⁺ insensitive red signal [R]) to allow for diffusional equilibration. We used a high concentration (1 mM) of medium-affinity Ca²⁺ indicator (K_d ~ 1.6 μ M for Fluo-5F), which is sufficient to dominate intracellular buffers (Sabatini et al., 2002).

Imaged spines were located on secondary and tertiary apical and basal dendrites within 160 μ m from the soma. Each imaging trial consisted of a series of nine sequential frames of 64 ms each: two frames with shutter closed to measure photomultiplier tube offsets, two frames after shutter opening to measure baseline fluorescence, and five frames following the uncaging stimulus to monitor [Ca²⁺]. Red and green fluorescence photons were separated using a dichroic mirror (565 nm) and bandpass filters (BG22 glass, 607/45 bandpass, Chroma). Photons were collected using photomultiplier tubes (Hamamatsu R3896). Epi- and transfluorescence signals were summed. For each spine, between five and ten trials were collected at 0.1 Hz, which did not cause rundown of uEPSC and spine [Ca²⁺] signals (data not shown).

Only spines that were clearly separated from other spines (>1 μ m away) were included in the analysis. Boxes were drawn surrounding the region of interest (ROI) containing the spine head. Calcium transient amplitude was calculated as the ratio of the change in Ca²⁺-sensitive green signal over the

Ca²⁺-insensitive red signal (dG/R), and calcium transient amplitude was measured as the signal in the first poststimulus frame minus the mean signal of the two baseline frames. To estimate saturation we compared dG/R with G/R_{max}, measured at saturating Ca²⁺ concentrations in a pipette (Yasuda et al., 2004). Under our conditions, average (dG/R)/(G/R_{max}) was 26% for persistent and new persistent spines and 13% for new spines. Saturation compresses the larger Δ [Ca²⁺] and therefore, in our case, would lead to an underestimation of the difference between new and control spines.

Estimation of Relative Spine Volume

Normalized spine volumes were calculated by dividing the peak spine brightness (measured as the mean of the pixels at the brightest point of the spine image), which is proportional to the spine volume (Nimchinsky et al., 2004), for each individual spine by the mean peak spine brightness of all persistent and new persistent spines (chronic imaging experiments; red channel; Alexa 594), or of all control spines (acute imaging experiments; green channel; GFP). Normalized spine volume estimates were well correlated with volume measurements of the same spines from retrospective SSEM ($r = 0.77$, $p < 0.01$; $n = 10$).

Photoactivation

Hippocampal pyramidal neurons were transfected with dsRedExpress (Clontech) and paGFP (Patterson and Lippincott-Schwartz, 2002) and imaged at 910 nm, 2–4 days after transfection. To identify new spines, two segments of secondary basal dendrites and two segments of secondary apical dendrites were imaged two times. Slices were maintained in culture medium and returned to the incubator (35°C) between imaging sessions. The second imaging time point was taken in ACSF. By imaging each dendrite twice, we were able to classify spines into two age groups: control (>1.5 hr) and new (<1.5 hr).

Immediately after the second time point, paGFP in individual dendritic spines was photoactivated by illuminating a box centered on the spine with a pulsed Ti:sapphire laser (Mai Tai, Spectra Physics) tuned to 810 nm (60–120 mW in the objective BFP). Each photoactivation trial consisted of 25 frames (64 \times 64 pixels, 128 ms): 10 frames of baseline, 14 frames following photoactivation, ~ 6 trials per spine at 10 s intervals. For each trial, time constants were calculated by fitting the decay of green fluorescence after photoactivation with a single exponential in a ROI surrounding the spine head, decay time constants were then averaged together for each spine. To insure adequate signal-to-noise in the exponential fit, only fluorescence transients whose amplitude reached greater than four times the standard deviation of the fluorescence in the baseline period were included in the analysis. Given the inaccuracy of measuring time constants significantly longer than the sampling period, estimates of τ were capped at 3500 ms.

Electron Microscopy

Immediately after imaging and recording, slices were fixed on ice in a solution of 0.2% glutaraldehyde and 2% paraformaldehyde in 0.1 M phosphate buffer (4°C, pH 7.4) for 2 hr, cryoprotected, antibody-stained (anti-GFP, Chemicon, AB3080), and prepped for EM (Supplemental Experimental Procedures). Resin embedded sections were viewed under a light microscope and the previously imaged GFP-labeled dendrites located. Serial thin sections (65 nm) were cut from this region and imaged at a magnification of 15,000 (Philips CM12, 80 kV). To visualize the dendrites in 3D, micrographs were aligned consecutively using Photoshop (Adobe) and exported to the Neurolucida software (MicroBrightfield). The dendrite and spines were traced so that the position of each spine identified in the serial EM images could be matched with the spines seen in the two-photon image.

Data Analysis and Statistics

Data were analyzed using custom software (Scheuss et al., 2006; Sobczyk et al., 2005) in Matlab (Mathworks, Natick, MA). Error bars represent standard error of the mean and significance was set at $p = 0.05$ (two-tailed t test, unless otherwise noted). r is the correlation coefficient and R^2 is the coefficient of determination.

Quantitative Model of Glutamate Receptor Distribution

Here we explore possible contributions of extrasynaptic receptors to uEPSCs. Assuming that extrasynaptic receptors are distributed uniformly throughout the dendritic and spine membranes, we calculate the fraction of total receptors that would have to be extrasynaptic to produce substantial responses in spines. We consider idealized spines with spherical heads and surface area A_{SH} . We assume that synaptic and extrasynaptic receptors are equally likely to be activated in the spine head membrane intersecting the uncaging volume. The total number of synaptic receptors is:

$$N_{Rs} = n_R b_s n_{spines} \quad (1)$$

where n_R is the total number of receptors in the spine, n_{spines} is the number of spines, and b_s is the fraction of receptors that are synaptic.

The density of extrasynaptic receptors in the membrane is

$$d_e = \frac{n_R(1 - b_s)}{a_A A_{SH}} \quad (2)$$

where a_A is the fraction of the spine head area intersecting the uncaging volume.

Thus the total number of extrasynaptic receptors is

$$N_{Re} = d_e A_{tot} = \frac{n_R(1 - b_s) A_{tot}}{a_A A_{SH}} \quad (3)$$

with A_{tot} being the total dendritic surface area including spines.

Finally, the fraction of total synaptic receptors relative to the total number of receptors is

$$\frac{N_{Rs}}{N_{Rs} + N_{Re}} = \left(1 + \frac{(1/b_s - 1) A_{tot}}{a_A n_{spines} A_{SH}}\right)^{-1} = \left(1 + \frac{(1/b_s - 1)}{a_A R_{SH/tot}}\right)^{-1} \quad (4)$$

with $R_{SH/tot}$ being the ratio of the total spine head surface area to total dendritic surface area including spines. We measured this ratio as $R_{SH/tot} = 0.0595$ from reconstructed dendritic segments (Figures 5 and S5; 0.0421 and 0.0823 in two different reconstructed segments). In Figure 2H, the fraction of total receptors that are synaptic is plotted against the fraction of receptors contributing to uncaging-evoked responses that are synaptic.

This analysis shows that if synaptic receptors contribute less than 80% to the uEPSC ($b_s < 0.8$), then less than 10% of all receptors would be synaptic ($N_{Rs}/N_{Rtot} < 0.1$), which contradicts reports on AMPA receptor distributions with immuno-EM (e.g., (Baude et al., 1995; Kharazia and Weinberg, 1999; Nusser et al., 1998). This argues strongly that new spines contain synapses and synaptic receptors.

SUPPLEMENTAL DATA

The Supplemental Data include Supplemental Experimental Procedures, Supplemental Discussion, seven figures, and one table, and can be found with this article online at [http://www.neuron.org/supplemental/S0896-6273\(08\)00965-3](http://www.neuron.org/supplemental/S0896-6273(08)00965-3).

ACKNOWLEDGMENTS

We would like to thank Barry Burbach, Sarah Parrish, and Catherine Zhang for help with experiments; Tim O'Connor and Aleks Sobczyk for programming; and Chris Harvey, Georgia Woods, Ryohei Yasuda, and Haining Zhong for critical reading of the manuscript. This work was supported by a Burroughs Wellcome Fund Career Award (K.Z.), the Human Frontier Science Program (V.S.), the Swiss National Science Foundation (G.K.), an NIH training grant (T.H.), and HHMI and NIH (K.S.).

Accepted: October 21, 2008

Published: January 28, 2009

REFERENCES

Alvarez, V.A., and Sabatini, B.L. (2007). Anatomical and physiological plasticity of dendritic spines. *Annu. Rev. Neurosci.* 30, 79–97.

Bailey, C.H., and Kandel, E.R. (1993). Structural changes accompanying memory storage. *Annu. Rev. Physiol.* 55, 397–426.

Baude, A., Nusser, Z., Molnar, E., McIlhinney, R.A., and Somogyi, P. (1995). High-resolution immunogold localization of AMPA type glutamate receptor subunits at synaptic and non-synaptic sites in rat hippocampus. *Neuroscience* 69, 1031–1055.

Beique, J.C., Lin, D.T., Kang, M.G., Aizawa, H., Takamiya, K., and Huganir, R.L. (2006). Synapse-specific regulation of AMPA receptor function by PSD-95. *Proc. Natl. Acad. Sci. USA* 103, 19535–19540.

Bekkers, J.M., and Stevens, C.F. (1989). NMDA and non-NMDA receptors are co-localized at individual excitatory synapses in cultured rat hippocampus. *Nature* 341, 230–233.

Bellone, C., and Nicoll, R.A. (2007). Rapid bidirectional switching of synaptic NMDA receptors. *Neuron* 55, 779–785.

Bloodgood, B.L., and Sabatini, B.L. (2005). Neuronal activity regulates diffusion across the neck of dendritic spines. *Science* 310, 866–869.

Bonhoeffer, T., and Yuste, R. (2002). Spine motility. Phenomenology, mechanisms, and function. *Neuron* 35, 1019–1027.

Bresler, T., Ramati, Y., Zamorano, P.L., Zhai, R., Garner, C.C., and Ziv, N.E. (2001). The dynamics of SAP90/PSD-95 recruitment to new synaptic junctions. *Mol. Cell. Neurosci.* 18, 149–167.

Buchanan, J., Sun, Y.A., and Poo, M.M. (1989). Studies of nerve-muscle interactions in *Xenopus* cell culture: fine structure of early functional contacts. *J. Neurosci.* 9, 1540–1554.

Busetto, G., Higley, M.J., and Sabatini, B.L. (2008). Developmental presence and disappearance of postsynaptically silent synapses on dendritic spines of rat layer 2/3 pyramidal neurons. *J. Physiol.* 586, 1519–1527.

Carter, A.G., and Sabatini, B.L. (2004). State-dependent calcium signaling in dendritic spines of striatal medium spiny neurons. *Neuron* 44, 483–493.

Colonnier, M. (1968). Synaptic patterns on different cell types in the different laminae of the cat visual cortex. An electron microscope study. *Brain Res.* 9, 268–287.

De Roo, M., Klausner, P., Mendez, P., Poggio, L., and Muller, D. (2008). Activity-dependent PSD formation and stabilization of newly formed spines in hippocampal slice cultures. *Cereb. Cortex* 18, 151–161.

Durand, G.M., Kovalchuk, Y., and Konnerth, A. (1996). Long-term potentiation and functional synapse induction in developing hippocampus. *Nature* 381, 71–75.

Engert, F., and Bonhoeffer, T. (1999). Dendritic spine changes associated with hippocampal long-term synaptic plasticity. *Nature* 399, 66–70.

Fiala, J.C., Spacek, J., and Harris, K.M. (2002). Dendritic spine pathology: cause or consequence of neurological disorders? *Brain Res. Brain Res. Rev.* 39, 29–54.

Friedman, H.V., Bresler, T., Garner, C.C., and Ziv, N.E. (2000). Assembly of new individual excitatory synapses: time course and temporal order of synaptic molecule recruitment. *Neuron* 27, 57–69.

Garaschuk, O., Yaari, Y., and Konnerth, A. (1997). Release and sequestration of calcium by ryanodine-sensitive stores in rat hippocampal neurones. *J. Physiol.* 502, 13–30.

Hall, B.J., and Ghosh, A. (2008). Regulation of AMPA receptor recruitment at developing synapses. *Trends Neurosci.* 31, 82–89.

Holtmaat, A., Wilbrecht, L., Knott, G.W., Welker, E., and Svoboda, K. (2006). Experience-dependent and cell-type-specific spine growth in the neocortex. *Nature* 441, 979–983.

Isaac, J.T., Nicoll, R.A., and Malenka, R.C. (1995). Evidence for silent synapses: implications for the expression of LTP. *Neuron* 15, 427–434.

Isaac, J.T., Oliet, S.H., Hjelmstad, G.O., Nicoll, R.A., and Malenka, R.C. (1996). Expression mechanisms of long-term potentiation in the hippocampus. *J. Physiol. (Paris)* 90, 299–303.

Jontes, J.D., and Smith, S.J. (2000). Filopodia, spines, and the generation of synaptic diversity. *Neuron* 27, 11–14.

- Jourdain, P., Fukunaga, K., and Muller, D. (2003). Calcium/calmodulin-dependent protein kinase II contributes to activity-dependent filopodia growth and spine formation. *J. Neurosci.* 23, 10645–10649.
- Kharazia, V.N., and Weinberg, R.J. (1999). Immunogold localization of AMPA and NMDA receptors in somatic sensory cortex of albino rat. *J. Comp. Neurol.* 412, 292–302.
- Knott, G.W., Quairiaux, C., Genoud, C., and Welker, E. (2002). Formation of dendritic spines with GABAergic synapses induced by whisker stimulation in adult mice. *Neuron* 34, 265–273.
- Knott, G.W., Holtmaat, A., Wilbrecht, L., Welker, E., and Svoboda, K. (2006). Spine growth precedes synapse formation in the adult neocortex in vivo. *Nat. Neurosci.* 9, 1117–1124.
- Kopeck, C.D., Real, E., Kessels, H.W., and Malinow, R. (2007). GluR1 links structural and functional plasticity at excitatory synapses. *J. Neurosci.* 27, 13706–13718.
- Lendvai, B., Stern, E.A., Chen, B., and Svoboda, K. (2000). Experience-dependent plasticity of dendritic spines in the developing rat barrel cortex in vivo. *Nature* 404, 876–881.
- Liao, D., Hessler, N.A., and Malinow, R. (1995). Activation of postsynaptically silent synapses during pairing-induced LTP in CA1 region of hippocampal slice. *Nature* 375, 400–404.
- Liao, D., Zhang, X., O'Brien, R., Ehlers, M.D., and Huganir, R.L. (1999). Regulation of morphological postsynaptic silent synapses in developing hippocampal neurons. *Nat. Neurosci.* 2, 37–43.
- Liu, X.B., Murray, K.D., and Jones, E.G. (2004). Switching of NMDA receptor 2A and 2B subunits at thalamic and cortical synapses during early postnatal development. *J. Neurosci.* 24, 8885–8895.
- Lohmann, C., Finski, A., and Bonhoeffer, T. (2005). Local calcium transients regulate the spontaneous motility of dendritic filopodia. *Nat. Neurosci.* 8, 305–312.
- Majewska, A., and Sur, M. (2003). Motility of dendritic spines in visual cortex in vivo: changes during the critical period and effects of visual deprivation. *Proc. Natl. Acad. Sci. USA* 100, 16024–16029.
- Maletic-Savatic, M., Malinow, R., and Svoboda, K. (1999). Rapid dendritic morphogenesis in CA1 hippocampal dendrites induced by synaptic activity. *Science* 283, 1923–1927.
- Matsuzaki, M., Ellis-Davies, G.C., Nemoto, T., Miyashita, Y., Iino, M., and Kasai, H. (2001). Dendritic spine geometry is critical for AMPA receptor expression in hippocampal CA1 pyramidal neurons. *Nat. Neurosci.* 4, 1086–1092.
- Matsuzaki, M., Honkura, N., Ellis-Davies, G.C., and Kasai, H. (2004). Structural basis of long-term potentiation in single dendritic spines. *Nature* 429, 761–766.
- Matus, A. (2005). Growth of dendritic spines: a continuing story. *Curr. Opin. Neurobiol.* 15, 67–72.
- Nagerl, U.V., Eberhorn, N., Cambridge, S.B., and Bonhoeffer, T. (2004). Bidirectional activity-dependent morphological plasticity in hippocampal neurons. *Neuron* 44, 759–767.
- Nagerl, U.V., Kostinger, G., Anderson, J.C., Martin, K.A., and Bonhoeffer, T. (2007). Protracted synaptogenesis after activity-dependent spinogenesis in hippocampal neurons. *J. Neurosci.* 27, 8149–8156.
- Nimchinsky, E.A., Yasuda, R., Oertner, T.G., and Svoboda, K. (2004). The number of glutamate receptors opened by synaptic stimulation in single hippocampal spines. *J. Neurosci.* 24, 2054–2064.
- Noguchi, J., Matsuzaki, M., Ellis-Davies, G.C., and Kasai, H. (2005). Spine-neck geometry determines NMDA receptor-dependent Ca²⁺ signaling in dendrites. *Neuron* 46, 609–622.
- Nusser, Z. (2000). AMPA and NMDA receptors: similarities and differences in their synaptic distribution. *Curr. Opin. Neurobiol.* 10, 337–341.
- Nusser, Z., Lujan, R., Laube, G., Roberts, J.D., Molnar, E., and Somogyi, P. (1998). Cell type and pathway dependence of synaptic AMPA receptor number and variability in the hippocampus. *Neuron* 21, 545–559.
- Okabe, S., Miwa, A., and Okado, H. (2001). Spine formation and correlated assembly of presynaptic and postsynaptic molecules. *J. Neurosci.* 21, 6105–6114.
- Park, M., Salgado, J.M., Ostroff, L., Helton, T.D., Robinson, C.G., Harris, K.M., and Ehlers, M.D. (2006). Plasticity-induced growth of dendritic spines by exocytic trafficking from recycling endosomes. *Neuron* 52, 817–830.
- Patterson, G.H., and Lippincott-Schwartz, J. (2002). A photoactivatable GFP for selective photolabeling of proteins and cells. *Science* 297, 1873–1877.
- Petralia, R.S., Esteban, J.A., Wang, Y.X., Partridge, J.G., Zhao, H.M., Wenthold, R.J., and Malinow, R. (1999). Selective acquisition of AMPA receptors over postnatal development suggests a molecular basis for silent synapses. *Nat. Neurosci.* 2, 31–36.
- Pologruto, T.A., Sabatini, B.L., and Svoboda, K. (2003). ScanImage: flexible software for operating laser scanning microscopes. *Biomed. Eng. Online* 2, 13.
- Racca, C., Stephenson, F.A., Streit, P., Roberts, J.D., and Somogyi, P. (2000). NMDA receptor content of synapses in stratum radiatum of the hippocampal CA1 area. *J. Neurosci.* 20, 2512–2522.
- Sabatini, B.L., Oertner, T.G., and Svoboda, K. (2002). The life cycle of Ca²⁺ ions in dendritic spines. *Neuron* 33, 439–452.
- Scheuss, V., Yasuda, R., Sobczyk, A., and Svoboda, K. (2006). Nonlinear [Ca²⁺] signaling in dendrites and spines caused by activity-dependent depression of Ca²⁺ extrusion. *J. Neurosci.* 26, 8183–8194.
- Segal, M. (2005). Dendritic spines and long-term plasticity. *Nat. Rev. Neurosci.* 6, 277–284.
- Skeberdis, V.A., Chevaleyre, V., Lau, C.G., Goldberg, J.H., Pettit, D.L., Suadicani, S.O., Lin, Y., Bennett, M.V., Yuste, R., Castillo, P.E., and Zukin, R.S. (2006). Protein kinase A regulates calcium permeability of NMDA receptors. *Nat. Neurosci.* 9, 501–510.
- Sobczyk, A., and Svoboda, K. (2007). Activity-dependent plasticity of the NMDA-receptor fractional Ca²⁺ current. *Neuron* 53, 17–24.
- Sobczyk, A., Scheuss, V., and Svoboda, K. (2005). NMDA receptor subunit-dependent [Ca²⁺] signaling in individual hippocampal dendritic spines. *J. Neurosci.* 25, 6037–6046.
- Stoppini, L., Buchs, P.A., and Muller, D. (1991). A simple method for organotypic cultures of nervous tissue. *J. Neurosci. Methods* 37, 173–182.
- Svoboda, K., Tank, D.W., and Denk, W. (1996). Direct measurement of coupling between dendritic spines and shafts. *Science* 272, 716–719.
- Takumi, Y., Ramirez-Leon, V., Laake, P., Rinivik, E., and Ottersen, O.P. (1999). Different modes of expression of AMPA and NMDA receptors in hippocampal synapses. *Nat. Neurosci.* 2, 618–624.
- Tovar, K.R., and Westbrook, G.L. (1999). The incorporation of NMDA receptors with a distinct subunit composition at nascent hippocampal synapses in vitro. *J. Neurosci.* 19, 4180–4188.
- Trachtenberg, J.T., Chen, B.E., Knott, G.W., Feng, G., Sanes, J.R., Welker, E., and Svoboda, K. (2002). Long-term in vivo imaging of experience-dependent synaptic plasticity in adult cortex. *Nature* 420, 788–794.
- Washbourne, P., Bennett, J.E., and McAllister, A.K. (2002). Rapid recruitment of NMDA receptor transport packets to nascent synapses. *Nat. Neurosci.* 5, 751–759.
- Wu, G., Malinow, R., and Cline, H.T. (1996). Maturation of a central glutamatergic synapse. *Science* 274, 972–976.
- Xiao, M.Y., Wasling, P., Hanse, E., and Gustafsson, B. (2004). Creation of AMPA-silent synapses in the neonatal hippocampus. *Nat. Neurosci.* 7, 236–243.
- Yasuda, R., Nimchinsky, E.A., Scheuss, V., Pologruto, T.A., Oertner, T.G., Sabatini, B.L., and Svoboda, K. (2004). Imaging calcium concentration dynamics in small neuronal compartments. *Sci. STKE* 2004, pl5.
- Yuste, R., and Bonhoeffer, T. (2001). Morphological changes in dendritic spines associated with long-term synaptic plasticity. *Annu. Rev. Neurosci.* 24, 1071–1089.

Zhou, Q., Homma, K.J., and Poo, M.M. (2004). Shrinkage of dendritic spines associated with long-term depression of hippocampal synapses. *Neuron* 44, 749–757.

Zito, K., Knott, G., Shepherd, G.M., Shenolikar, S., and Svoboda, K. (2004). Induction of spine growth and synapse formation by regulation of the spine actin cytoskeleton. *Neuron* 44, 321–334.

Ziv, N.E., and Smith, S.J. (1996). Evidence for a role of dendritic filopodia in synaptogenesis and spine formation. *Neuron* 17, 91–102.

Zuo, Y., Yang, G., Kwon, E., and Gan, W.B. (2005). Long-term sensory deprivation prevents dendritic spine loss in primary somatosensory cortex. *Nature* 436, 261–265.